Lumped battery models predict cell heterogeneity and effective temperature when thermal parameters are identified from electrical data

Mark Blyth*[1,2] and Alastair Hales[1,2]

[1]University of Bristol, UK
[2]The Faraday Institution, UK

May 13, 2025

Abstract

Battery design, management, and control uses coupled electrical and thermal models to predict cell performance. Computational constraints mean lumped models are used, where temperature and charge are assumed to be spatially uniform. Accuracy is not guaranteed, as electrochemical systems generate heat which drives temperature gradients. These change the cell behaviour, but are not described by lumped models. Accuracy is further limited by the difficulties in finding good thermal parameters. To address these challenges, we first demonstrate a simple experimental method for obtaining thermal parameters. Our thermal parameterisation method works by maximising the voltage accuracy of an electrothermal model. This allows thermal parameters to be found quickly and easily, using only voltage-based cell cycling data. We then show that lumped models can perform accurately on cells with temperature gradients. We first define the correct lumped-model temperature for a cell with a thermal gradient, then show that our thermal parameters lead to this temperature. To do so, an explicit distributed cell model is derived and analysed, which consists of parallel connected Thevenin circuits. This is used to construct a formula for effective temperature — the temperature a uniform cell must be at, to show the same impedance, and hence, electrical behaviours, as a heterogeneous cell. Our thermal parameters are shown to produce effective temperature predictions, meaning the lumped model will match the impedance of a heterogeneous cell. Our results demonstrate that lumped models can be used with confidence, even on large-scale, heterogeneous systems, provided the thermal parameters are calibrated using voltage data.

1 Background

Temperature is an immensely important variable in battery systems. Electrochemical kinetics vary with temperature, which drives changes in performance characteristics such as accessible capacity and rate capability. Temperature extremes can damage cells, by accelerating unwanted side reactions [1] or causing thermal runaway [2]. A detailed understanding of cell heating, cooling, and temperature dependency is therefore essential for the design, control, and safe operation of battery packs. While thermal modelling is very well understood, two key challenges emerge when combining it with electrochemical systems.

The first challenge covers heterogeneous effects [3, 4], whereby cell performance changes due to the impacts of spatially varying, non-uniform temperature distributions. Heat is generated within a cell during operation [5]. Thermal management systems are used to remove this heat, to ensure cell temperature remains within a safe range. The combination of heat generation and removal causes temperature gradients to form. Since cell impedance varies with temperature and state of charge [6, 7], temperature gradients lead to non-uniform current densities, which in turn produces spatial variations in the amount of charge stored across a cell or battery [8, 9]. Notably, these effects cannot be volume-averaged away — a heterogeneous cell will behave differently to an equivalent idealised cell at a uniform, volume-averaged temperature [10].

The second key challenge is that while thermal models are well understood, accurate thermal parameters are often difficult and expensive to obtain. Typically, heat capacities would be found using calorimetry experiments [11, 12]. This is easily achievable for single cells, however it become impractical for larger systems such as modules and packs. Thermal testing at module and pack scale is required, due

to the impacts of thermal pathways such as bus-bars and module casings. Heat transfer coefficients are difficult to measure, and instead estimates are typically made from known correlations. Consequently, the resulting parameters are unlikely to be truly representative of the battery system of interest, which impairs model-based temperature estimation. Even if perfect thermal parameters were available, their usage in a lumped model would yield predictions of volume-averaged cell temperature, which, as noted, is not the correct measurement for use in electrical models [10].

Cell behaviours can be studied using detailed models which capture coupled, spatially varying thermal and electrical behaviours. These so-called distributed models are regularly used for investigating heterogeneous battery systems, and represent full cells or packs as multiple electrically and thermally connected units, to capture the full range of heterogeneous effects inside the system [13]. Previous studies use this modelling approach to investigate topics such as tab and cell design [14, 15] and thermal management strategies [16, 17]. Distributed models are useful for cell design, however they are impractical for online estimation and control due to their large computational requirements; likewise, pack-scale design optimisation becomes challenging due to the computational demands involved. More often, lumped models are used, which provide a significant computational speed-up by discounting heterogeneous effects. The accuracy of this approach is limited by the inability to capture heterogeneity effects, and the difficulty in obtaining good thermal parameters.

Given these challenges, it is desirable to build cell models that are computationally lightweight, capture heterogeneous dynamics, and provide high accuracy without requiring difficult and expensive thermal parameterisation. Here, we address these two important and closely linked challenges. In section 2 we provide a simple method for identifying thermal parameters from electrical data, without the need for any specialised thermal testing equipment. Our method extracts parameters from voltage measurements, by exploiting the links between thermal parameters, cell temperature, and electrical responses. Laboratory experiments demonstrate that this method is feasible and produces useful results. Our second contribution, in section 3, defines the correct temperature measure for lumped modelling of heterogeneous cells, and shows that our thermal modelling methods produce this temperature. Previous work [18, 19, 20, 21] defines the effective temperature of a cell as the temperature a uniform cell needs to be at, to show the same impedance — and therefore, electrical behaviours — as a heterogeneous cell. We develop this idea as a modelling tool, by showing how the effective temperature of a cell can be calculated. Modelling work shows that a thermal model produced using our parameterisation technique will predict the effective temperature of a cell, and outperform conventional methods when used in electrical models. To perform this analysis, an explicit distributed cell model is derived, which is the first closed-form model of an electrothermally coupled, heterogeneous cell in the literature. Our work demonstrates the value of these explicit models, both for more efficient simulations, and for formal mathematical analysis. More generally, our findings allow lumped models to be used with confidence — cell heterogeneity can be rigorously accounted for using effective temperature, and models for predicting effective temperature can be easily constructed using our validated parameterisation protocols.

2 Developing a thermal model parameterisation pipeline

It is commonly accepted that the most effective model for battery management will have the lowest voltage prediction error. Thermal models impact voltage predictions, because of the influence of temperature on cell impedance. Consequently, thermal parameters should also be tuned to minimise voltage prediction error. This differs from commonly employed methods in the literature, where voltage predictions are ignored and models are tested on surface temperature measurements [22, 23, 24], which will offer sub-par predictions of cell impedance [10]. We now show how thermal parameters can be identified by minimising the voltage prediction errors of a coupled electrothermal model, and develop a novel thermal parameterisation method based only on electrical data.

First, a cell model is created and validated with standard laboratory experiments, to predict the electrical behaviours of a cell at some known, uniform temperature. Next, the same cell is tested under conditions where its temperature is allowed to vary. The electrical model is now coupled to a thermal model, which is used to predict the varying cell temperature. Voltage accuracy will be maximised when the temperature estimates of the thermal model are correct, as the impedance of the model will then match that of the real cell. Thermal parameters are therefore identified, by tuning them to maximising the voltage accuracy of the model.

Experimental results are reported which illustrate how this method is applied in practice, and demonstrate the viability of the approach. The parameters identified using our method are validated against literature data, and shown to compare favourably. Testing with our approach removes the costs and

Temperature [°C]	5	10	15	25	40
Model RMSE [mV]	12.0	10.2	9.50	10.4	16.2

Table 1: Model validation results. Electrical model root-mean-square errors are calculated on a WLTP drive-cycle at each tested temperature, showing good model performance at all temperatures. RMSE values are notably increased by the larger prediction errors at low states-of-charge, as illustrated in Fig. 1.

difficulties of traditional thermal tests, and ensures that the modelled cell temperatures are as accurate as possible for use in an electrical model. Section 3 will then demonstrate that the resulting temperature predictions are the correct choice for lumped modelling of heterogeneous cells, and develops a theory of effective temperature to explain the success of this parameterisation strategy.

2.1 Part 1: building an electrical model

Initially, a constant-temperature electrical model is fitted to voltage data; section 2.2 then employs a thermal sub-model, and tunes its parameters to maximise voltage prediction accuracy. A standard n-RC Thevenin equivalent-circuit model [25] is chosen. Thevenin models are used extensively throughout the literature due to their ease of parameterisation, and potential for high accuracy. Furthermore, the model structure is simple enough for analytical study, which can become challenging with physics-based models.

The model has terminal voltage v_{batt} [V], nominal cell capacity Q_{nom} [A s], series resistance R_0^{lumped} [Ω], polarisation resistances R_i^{lumped} [Ω] and capacitances C_i^{lumped} [F]. Each RC branch has a polarisation overpotential v_{rc_i} [V], for $i \in \{1, \dots, n_{\text{rc}}\}$. The cell has a state-of-charge SOC, and open-circuit voltage v_{oc} [V]. Current $I(t)$ [A] is taken as positive during charge. The electrical problem will be coupled to a lumped thermal model, with thermal mass c [J K^{-1}], heat transfer coefficient h [W K^{-1}], temperature T [°C], and far-field temperature T_∞ [°C]. Heat generation $q(t)$ [W] comes from Joule heating and, optionally, entropic heating [5]. Dynamics are governed by

$$\frac{\mathrm{d}}{\mathrm{d}t}SOC = \frac{I(t)}{Q_{\text{nom}}}\,, \tag{1}$$

$$\frac{\mathrm{d}v_{\text{rc}_i}}{\mathrm{d}t} = \frac{1}{C_i(T, SOC)}\left(I(t) - \frac{v_{\text{rc}_i}}{R_i(T, SOC)}\right)\,, \tag{2}$$

$$v_{\text{batt}}(t) = v_{\text{oc}}(T, SOC) + I(t)R_0(T, SOC) + \sum_{i=1}^{n_{\text{rc}}} v_{\text{rc}_i}\,, \tag{3}$$

$$\frac{\mathrm{d}T}{\mathrm{d}t} = \frac{1}{c}\left(q(t) - h(T - T_\infty)\right)\,, \tag{4}$$

$$q(t) = I^2(t)R_0(T, SOC) + \sum_{i=1}^{n_{\text{rc}}} \frac{v_{\text{rc}_i}^2}{R_i(T, SOC)} - I(t)T(t)\frac{\partial v_{\text{oc}}}{\partial T} \tag{5}$$

for time t [s]. The thermal sub-model (Eqs. (4)–(5)) is initially ignored during the electrical parameterisation experiments, and cell temperature is taken from the experimental conditions.

Experiments are conducted on pouch cells manufactured by LiFun, with a graphite anode and NMC 622 cathode. Cell dimensions are 62 mm (L) × 48 mm (W) × 6 mm (T), with both tabs at the top of the cell. Nominal capacity is stated as 1.8 Ah, but taken here as 2.2 Ah based on estimates from cycling data. Careful thermal control is required for producing a lumped, isothermal electrical model. To achieve this, cell surfaces are maintained at a constant temperature using a custom-built thermal control system, using thermistors for temperature measurements, Peltier elements to heat and cool the cell surfaces, and a PID feedback loop for control. Peliter elements reject heat into a liquid cooling block, which is connected to an external chiller loop. Active thermal control is deemed superior to climate chamber testing, as the cell surface temperature is kept constant; temperature variations would be expected in a climate chamber, due to the limitations of convective cooling.

Parameterisation of the electrical model involves finding values for the open-circuit voltage v_{oc}, resistances R_0 and R_i, and capacitances C_i as a function of state-of-charge and temperature. Pulse-discharge tests are used to extract these parameters. This has reached a high state of maturity in the literature [26, 27, 28, 29, 30, 31], and pre-built software tools are available [32, 33]. Pulses involve discharging the cell at 0.4 C for 6 minutes, then allowing it to rest for 2 h to return to open-circuit voltage. Open-circuit voltage curves $v_{\text{oc}}(SOC)$ are found from the relaxation voltages reached at the end of each rest.

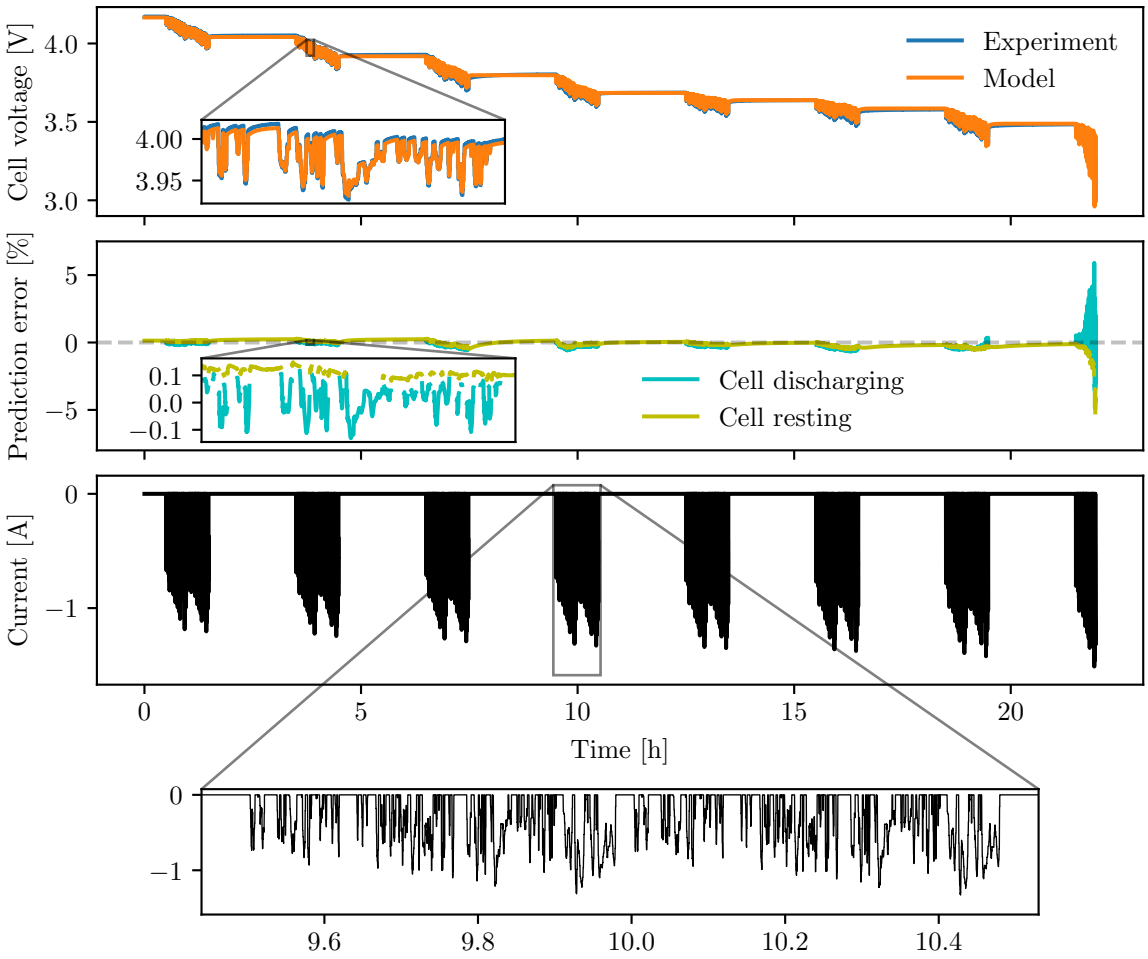

Figure 1: Validation of the fitted electrical model at 25 °C. Model predictions are seen to match with experimental data to a high degree of accuracy, except at low states of charge.

The electrical sub-model given in Eqs. (1)–(3) is fitted to each pulse individually, by using a nonlinear least squares solver to identify parameters R_0, R_1, R_2, C_1, and C_2. Parameters are fitted to data from the pulse, and not during the relaxation when current is zero, so that they are representative of operational cell behaviour. Parameterisation is repeated across the full state-of-charge range, and at various temperatures. Functional parameters $R_0(T, SOC)$ etc. are then constructed by interpolating the parameters over temperature and state-of-charge. Cells are recharged with a C/3 constant-current charge, followed by a constant voltage hold at 4.2 V until current drops below 0.09 C; this is always performed at 25 °C to ensure consistency between tests.

Electrical modelling is completed by validating at each tested temperature. Electrical predictions are compared against experimentally measured voltages, for a power-based WLTP drive cycle experiment, recorded under careful thermal control. Root-mean-square model errors are given in Table 1. An example validation procedure is shown in Fig. 1, which demonstrates that the model achieves a good prediction accuracy across most of the data range. Model errors are increased by a reduction in prediction accuracy at low states of charge, which is caused by parameterisation challenges from the rapid parameter changes in this region.

2.2 Part 2: fitting a thermal model

An electrical model has now been built and validated, which provides an accurate description of cell voltage at some known, uniform temperature. Next, the thermal sub-model (Eqs. (4)–(5)) is included, and thermal parameters are tuned to maximise voltage prediction accuracy. Thermal parameters are identifiable from electrical data because a minimal voltage error requires a correct impedance estimate from the electrical model, and the impedance estimate will only be correct when the cell temperature is

correct. This requires a suitable thermal testing experiment, developed here. Section 3 then justifies the results by explaining what the 'correct' lumped temperature measurement is, for a heterogeneous cell operating with a temperature distribution.

The same cell is now cycled under realistic operating conditions, which in general should be designed to represent the cell's usage environment. This may include pack-design choices such as stacks of cells or modules, and forced convection or cold-plate cooling. Here, cold-plate cooling is used; cells are operated without Peltier-based thermal control, but the water cooling loop remains switched on to allow heat rejection. The lack of precise temperature control means the cell will exhibit significant heterogeneity and temperature changes, and as a result, the voltage responses $v_{\text{hetero}}(t)$ will differ to those predicted by the parameterised electrical model. To account for this, the electrical model is coupled to a thermal model, whose parameters are identified from cycling data.

Cycling data can be carefully designed to provide as much information as possible for the fitting process. Eq. (4) with a constant heat generation rate $q(t)$ would reach a steady-state temperature of q/h °C above ambient temperature T_∞. The time taken to reach this steady-state temperature is governed by thermalisation timescale, c/h s. As such, thermal mass c only influences temperature transients, so the drive cycle should induce regular changes to the cell temperature to allow accurate identification of c. This is readily achievable by varying current draw. Our thermal-test drive cycle alternates periodically between a higher and lower discharge current to induce regular transients in the cell temperature. Cells are discharged with a current that alternates between 0.5 C and 0.8 C every 500 s in this work, however current draws and switching time can be varied according to the parameters and thermalisation timescales of the tested cells.

To fit the thermal parameters, the lumped electrothermal model of Eqs. (1)–(5) is simulated, yielding predictions $v_{\text{lumped}}(t)$ and prediction error $\|v_{\text{lumped}}(t) - v_{\text{hetero}}(t)\|^2$. A numerical optimiser is used to update the parameter estimates for c and h, thus parameterising the thermal model by solving

$$\min_{c,h} \|v_{\text{lumped}}(t) - v_{\text{hetero}}(t)\|^2. \tag{6}$$

A gradient-free Nelder-Mead optimisation algorithm is found to perform well here. The use of a minimisation-based approach is necessarily robust against voltage prediction errors in the electrical model, as an error-minimum will always exist. Optimisation algorithms require an initial solution guess; this could be obtained from literature estimates of the thermal mass and heat transfer coefficient, however we instead choose initial conditions from a grid search method, to ensure the fitted parameters are free from input and bias from the experimenters. The grid search is performed over a broad range of c and h to find sensible initial conditions, which are then used as a starting point for the Nelder-Mead algorithm.

Literature data from cylindrical cells give jellyroll density ρ as 2682 kg m^{-3}, and specific heat capacity c_p as 887 J kg^{-1} K^{-1}. Using these data for the cell tested here gives $c = \rho c_p \mathcal{V} = 42.5$ J K^{-1}, where $\mathcal{V}$ is cell volume. A wide range of convection coefficients are stated in the literature, ranging from 10 W m^{-2} K^{-1} for air cooling, to 2000 W m^{-2} K^{-1} for single-phase immersion cooling [34]. Our indirect liquid cooling setup is expected to have a reasonably high heat transfer coefficient; taking a mid-range estimate of 500 W m^{-2} K^{-1} gives a heat transfer coefficient of $h = 2.97$ W K^{-1} for two-sided cooling of a cell with our given dimensions. To cover a realistic range of possible parameter values, a grid search is conducted over a 20×20 equispaced grid, with $c \in [1, 200]$ and $h \in [0.1, 4]$. Optimisation using the grid-search and Nelder-Mead procedures give thermal parameters of $c = 42.9$ J K^{-1} and $h = 3.59$ W K^{-1}, comparing very favourably to literature estimates. This demonstrates that our experimental method is practically achievable, and capable of finding meaningful and useful thermal parameters. The wider value and benefits of this method shall be explored in the next section.

3 Effective temperature of heterogeneous cells

We now introduce the second major contribution of this work, whereby we show that the performance of a heterogeneous cell can be described accurately using lumped models. A methodology has been introduced for extracting the parameters of a lumped thermal model. As noted, real cells are heterogeneous and will operate under temperature gradients, and volume-averaged temperatures are not the correct way of representing this [10]. A sensible lumped-model temperature is known to exist [18, 19], referred to here as effective cell temperature, however the literature has not studied how this temperature can be calculated. We therefore introduce a method for calculating effective temperature, which in turn rigorously shows that a lumped model can be used for describing heterogeneous cells. The analysis requires a heterogeneous

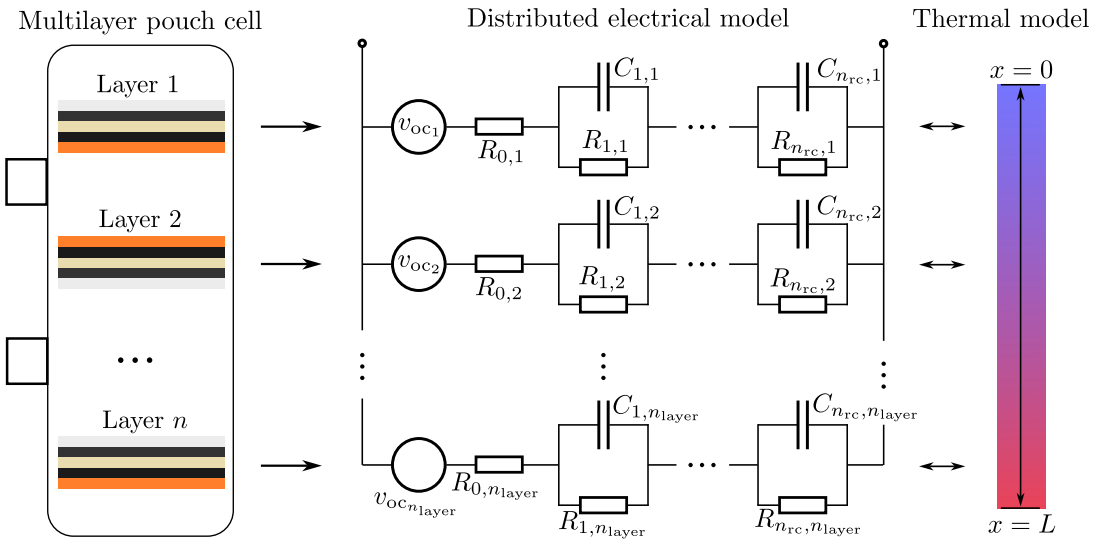

Figure 2: Diagram of the heterogeneous model developed here. Pouch cells consist of stacked layers of current collectors, active material, and separators. Each layer of a pouch cell, and of the model, acts as its own cell, and is connected in parallel to every other layer. The electrical problem is coupled to a 1d thermal model.

cell model. Existing heterogeneous cell models are pitched as software simulators, which are not suitable for formal analysis. Therefore, in section 3.1 we derive an explicit model of a heterogeneous cell, which in itself is an important contribution to the literature. Once an appropriate model has been established, section 3.2 then show how the effective temperature of a cell can be calculated from its temperature and state-of-charge gradients. This gives the correct temperature measurement to use when applying lumped models to heterogeneous cells. Section 3.3 demonstrates that the thermal parameterisation procedures developed in section 2 result in a thermal model that predicts effective temperature. This justifies the use of our thermal parameterisation methods, explains how and why lumped models can be applied when faced with heterogeneity, and confirms that our methods produce lumped models which are appropriate for heterogeneous cells.

3.1 An explicit model of a heterogeneous cell

While the dynamics of parallel-connected cells is known [35], a full mathematical description of a distributed cell model is missing in the literature. We now address this gap by deriving an explicit distributed cell model, capturing the coupling between temperature distributions and electrical dynamics. We describe a one-dimensional temperature gradient, as it represents the simplest possible description of a spatially heterogeneous cell, however results can easily be extended to higher dimensions. Our distributed model generalises the lumped model of Eqs. (1)–(5), to include spatial variations of cell states. Spatial effects are captured using a collection of parallel-connected equivalent circuit branches, as sketched in Fig. 2. Each individual circuit-branch is interpreted as a single layer (or collection of adjacent layers) within a pouch cell[1]. Heat generation in each cell-layer is found from the ohmic losses of an electrical model. Each electrical model branch tracks the state-of-charge, current density, and polarisation overpotentials of the respective cell layer. Thermal effects are described with a discretised heat equation, coupled to the electrical problem. Together, these provide all the necessary information to understand how the heterogeneous cell behaves.

We first introduce the electrical problem. Consider the jth layer of the model, with state-of-charge SOC_j, temperature T_j, and layer-current I_j. Each layer has a capacity of $Q_{\mathrm{nom}}/n_{\mathrm{layer}}$, and hence, layerwise state-of-charge evolves as

$$\frac{\mathrm{d}}{\mathrm{d}t} SOC_j(t) = n_{\mathrm{layer}} \frac{I_j(t)}{Q_{\mathrm{nom}}} \,. \tag{7}$$

The resistances and capacitances of each layer will differ to those of the overall cell. A components-in-

[1]The model and results can also be taken to represent parallel-connected cells in a battery module.

parallel argument gives each layer's resistance and capacitance as

$$R_0^{\text{layer}} = R_0^{\text{lumped}}(T, SOC)\ n_{\text{layer}}\ , \tag{8}$$

$$R_i^{\text{layer}} = R_i^{\text{lumped}}(T, SOC)\ n_{\text{layer}}\ , \tag{9}$$

$$C_i^{\text{layer}} = C_i^{\text{lumped}}(T, SOC)\ /\ n_{\text{layer}} \tag{10}$$

for $i \in \{1, \ldots, n_{\text{rc}}\}$. Such scalings are used as standard in distributed models [36, 16]. This scaling is explicitly included in the following derivation, so that functional parameters R_0 etc. are identical to those used in the lumped model; an alternative would be to define new functional parameters $\tilde{R}_0 = R_0 n_{\text{layer}}$ etc., representing the component values of each individual layer.

Kirchoff's voltage law dictates that the overall cell terminal voltage v_{batt} is related to layer current I_j by

$$v_{\text{batt}}(t) = v_{\text{oc}}\left(SOC_j\left(t\right)\right) + I_j(t) n_{\text{layer}} R_0\left(T_j\left(t\right), SOC_j\left(t\right)\right) + \sum_{i=1}^{n_{\text{rc}}} v_{\text{rc}_{i,j}}(t) \tag{11}$$

for each layer j. (For ease of notation, we now drop explicit dependencies t, $T_j\left(t\right)$, etc..) Rearranging Eq. (11), the current through layer j is

$$I_j = \frac{1}{n_{\text{layer}} R_{0,j}} \left(v_{\text{batt}} - v_{\text{oc}_j} - \sum_{i=1}^{n_{\text{rc}}} v_{\text{rc}_{i,j}} \right)\ . \tag{12}$$

By Kirchoff's current law, the current $I(t)$ through the full cell is related to the layer currents I_j by

$$I = \sum_{j=1}^{n_{\text{layer}}} I_j\ . \tag{13}$$

Substituting the layer currents from Eq. (12) into Eq. (13), and rearranging the result for terminal voltage v_{batt}, yields the output equation for a heterogeneous system as

$$v_{\text{batt}}(t) = \frac{\sum_{j=1}^{n_{\text{layer}}} \frac{v_{\text{oc}_j}}{R_{0,j}}}{\sum_{j=1}^{n_{\text{layer}}} \frac{1}{R_{0,j}}} + I(t) \left(\frac{n_{\text{layer}}}{\sum_{j=1}^{n_{\text{layer}}} \frac{1}{R_{0,j}}} \right) + \frac{\sum_{j=1}^{n_{\text{layer}}} \frac{\sum_{i=1}^{n_{\text{rc}}} v_{\text{rc}_{i,j}}}{R_{0,j}}}{\sum_{j=1}^{n_{\text{layer}}} \frac{1}{R_{0,j}}}\ , \tag{14}$$

where $R_{0,j} := R_0\left(T_j\left(t\right), SOC_j\left(t\right)\right)$ and $v_{\text{oc}_j} := v_{\text{oc}}\left(SOC_j\left(t\right)\right)$.

As with the homogeneous model, $v_{\text{rc}_{i,j}}$ — the overpotential across the ith RC pair of layer j — evolves according to

$$\frac{\mathrm{d}}{\mathrm{d}t} v_{\text{rc}_{i,j}}\left(t\right) = \frac{n_{\text{layer}}}{C_{i,j}} \left(I_j - \frac{v_{\text{rc}_{i,j}}}{n_{\text{layer}} R_{i,j}} \right)\ , \tag{15}$$

following the usual notation, whereby $R_{i,j} = R_i\left(T_j\left(t\right), SOC_j\left(t\right)\right)$ and $C_{i,j} = C_i\left(T_j\left(t\right), SOC_j\left(t\right)\right)$. Eq. (12) can be substituted into Eq. (15) to give the dynamics of each RC overpotential in terms of known quantities. The overpotential of the ith RC pair of the jth layer is thus given by

$$\frac{\mathrm{d}}{\mathrm{d}t} v_{\text{rc}_{i,j}} = \frac{1}{C_{i,j}} \left(\frac{v_{\text{batt}} - v_{\text{oc}_j} - \sum_{i=1}^{n_{\text{rc}}} v_{i,j}}{R_{0,j}} - \frac{v_{\text{rc}_{i,j}}}{R_{i,j}} \right)\ , \tag{16}$$

with v_{batt} as per Eq. (14). This gives the full system dynamics of the electrical problem as

$$\begin{cases} \dfrac{\mathrm{d}}{\mathrm{d}t} SOC_j(t) = \dfrac{v_{\text{batt}} - v_{\text{oc}_j} - \sum_{i=1}^{n_{\text{rc}}} v_{i,j}}{R_{0,j} Q_{\text{cell}}}\ , & j \in [1, \ldots, n_{\text{layer}}] \\ \dfrac{\mathrm{d}}{\mathrm{d}t} v_{\text{rc}_{i,j}}(t) = \dfrac{1}{C_{i,j}} \left(\dfrac{v_{\text{batt}} - v_{\text{oc}_j} - \sum_{i=1}^{n_{\text{rc}}} v_{i,j}}{R_{0,j}} - \dfrac{v_{\text{rc}_{i,j}}}{R_{i,j}} \right)\ , & i \in [1, \ldots, n_{\text{rc}}]\ , \\ v_{\text{batt}}(t) = \dfrac{1}{\sum_{j=1}^{n_{\text{layer}}} \frac{1}{R_{0,j}}} \left(\sum_{j=1}^{n_{\text{layer}}} \dfrac{v_{\text{oc}_j}}{R_{0,j}} + n_{\text{layer}} I(t) + \sum_{j=1}^{n_{\text{layer}}} \dfrac{\sum_{i=1}^{n_{\text{rc}}} v_{\text{rc}_{i,j}}}{R_{0_{i,j}}} \right)\ . \end{cases} \tag{17}$$

The thermal problem is now introduced. Consider a cell of thickness L [m], with line density ρ [kg m^{-1}] and constant, isotropic specific heat capacity c_p [J K^{-1} kg^{-1}] and thermal diffusivity $\mathcal{D}$ [m^2 s^{-1}].

For a localised heat generation rate $\tilde{q}(x,t)$ [W m^{-1}], the temperature profile $T(x,t)$ [°C] is governed by

$$\begin{cases} \dfrac{\partial T}{\partial t} = \mathcal{D}\dfrac{\partial^2 T}{\partial x^2} + \dfrac{1}{\rho c_p}\tilde{q}(x,t) \ , \\ \dfrac{\partial T}{\partial x}\Big|_{x=0} = h_0\big(T(0,t) - T_\infty\big) \ , \\ \dfrac{\partial T}{\partial x}\Big|_{x=L} = -h_L\big(T(L,t) - T_\infty\big) \ , \end{cases} \tag{18}$$

for far-field temperature T_∞ [°C], and coefficients h_0 and h_L [m^{-1}], where $h = \lambda/k$ for convection coefficients $\lambda \in \{\lambda_0, \lambda_L\}$ [W m^{-2} K^{-1}], and cell thermal conductivity k [W m^{-1} K^{-1}]. Consider the discretisation of $[0, L]$ into nodes $x_1, \ldots, x_{n_{\text{nodes}}}$. We choose to associate each node of the thermal problem with a layer of the electrical problem, and hence, $n_{\text{nodes}} = n_{\text{layer}}$. Applying a method-of-lines discretisation [37] yields

$$\begin{cases} \dfrac{\mathrm{d}T_1}{\mathrm{d}t} = \mathcal{D}\left(\dfrac{T_2 - T_1}{\Delta x^2} + h_0\dfrac{T_1 - T_\infty}{\Delta x}\right) + \dfrac{1}{\rho c_p}q_1(t) \ , \\ \dfrac{\mathrm{d}T_j}{\mathrm{d}t} = \mathcal{D}\dfrac{T_{j-1} - 2T_j + T_{j+1}}{\Delta x^2} + \dfrac{1}{\rho c_p}q_j(t) \ , \\ \dfrac{\mathrm{d}T_{n_{\text{layer}}}}{\mathrm{d}t} = \mathcal{D}\left(\dfrac{T_{n_{\text{layer}}-1} - T_{n_{\text{layer}}}}{\Delta x^2} + h_L\dfrac{T_{n_{\text{layer}}} - T_\infty}{\Delta x}\right) + \dfrac{1}{\rho c_p}q_{n_{\text{layer}}}(t) \ , \end{cases} \tag{19}$$

for $T_j = T(x_j, t)$, $\Delta x = L/(n_{\text{layer}} - 1)$, where

$$q_j(t) = \frac{1}{\Delta x}\int_{x_j}^{x_{j+1}} \tilde{q}(x,t)\ \mathrm{d}x$$

[W m^{-1}] is the average heat generation rate within finite-volume (node) j. This is obtained from the irreversible heat generation of the jth electrical layer, as

$$q_j = \frac{1}{\Delta x}\left(I_j^2 R_{0,j} + \sum_{i=1}^{n_{\text{rc}}} \frac{v_{\text{rc}_{i,j}}^2}{R_{i,j}}\right) \ . \tag{20}$$

Reversible heating is omitted here as it is not relevant to our following analysis. Nevertheless, it could trivially be included through the addition of an entropy term in Eq. (20) [5].

The heterogeneous cell model is fully defined by the combination of the electrical sub-model, Eqs. (17); the thermal sub-model, Eqs. (19); the heat generation rate, Eq. (20); and a suitable set of initial conditions.

3.2 Calculating the effective temperature of a heterogeneous cell

Eqs. (17) offers a range of important insights into heterogeneous cell dynamics, which are exploited here to derive an explicit formula for the effective temperature of a cell. The resulting formula produces a single measure to describe heterogeneous cell temperatures, based on the overall impact of temperature and state-of-charge distributions on cell behaviour. In turn, this allows the performance of a heterogeneous cell to be accurately described using simple, lumped models. Effective temperature is required because volume-averaged temperature is the incorrect temperature measure for a heterogeneous cell [10]; instead, effective temperature may be interpreted as the resistance-weighted average temperature of a cell.

The various terms of the output equation in Eq. (17) can be interpreted as

$$v_{\text{batt}}(t) = \underbrace{\frac{\sum_{j=1}^{n_{\text{layer}}} \frac{v_{\text{oc}_j}}{R_{0,j}}}{\sum_{j=1}^{n_{\text{layer}}} \frac{1}{R_{0,j}}}}_{\text{Heterogeneous OCV}} + \underbrace{\left(\frac{n_{\text{layer}}}{\sum_{j=1}^{n_{\text{layer}}} \frac{1}{R_{0,j}}}\right)}_{\text{Emergent series resistance}} I(t) + \underbrace{\frac{\sum_{j=1}^{n_{\text{layer}}} \frac{\sum_{i=1}^{n_{\text{rc}}} v_{\text{rc}_{i,j}}}{R_{0,j}}}{\sum_{j=1}^{n_{\text{layer}}} \frac{1}{R_{0,j}}}}_{\text{Weighted transient overpotentials}} \ . \tag{21}$$

We now focus on the emergent resistance of the heterogeneous cell; effective temperature is the temperature a lumped model or homogeneous cell must be at, to show this resistance. Here, cell resistance is taken to mean series resistance R_0, as it is the easiest of the resistances to identify accurately in parameterisation experiments, and can be estimated during online cell operation. This approach also

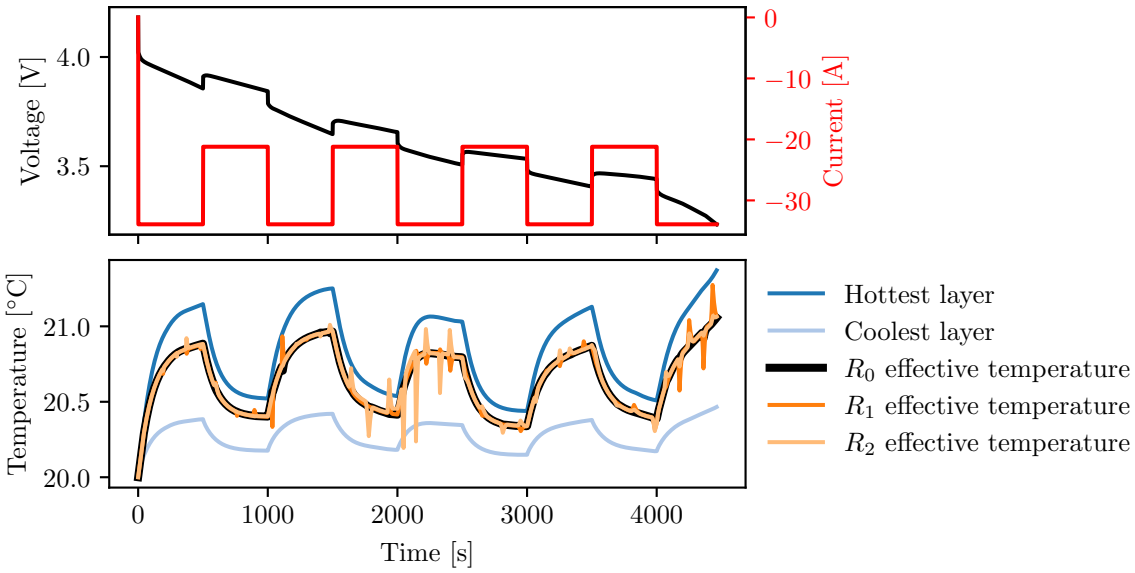

Figure 3: Drive cycle and associated synthetic data used to study effective temperature. Top: a model cell is discharged with currents alternating between 0.5 C and 0.8 C every 500 s. Bottom: temperatures of the hottest and coldest layers of the model-cell, and effective temperature as calculated with each resistor.

complements online methods using electrochemical impedance spectroscopy, from which the cell series resistance can be found [20, 38]. Nevertheless, it is possible to perform a similar derivation using polarisation resistances R_i, instead of cell series resistance R_0; this would yield the same result, only with R_i in place of R_0. This is confirmed in Fig. 3, which shows the cell test studied in the following section. Effective temperature is calculated using both series and polarisation resistances, which are seen to give the same results. However, the polarisation resistance results show small random fluctuations, which are thought to arise from challenges in accurately parameterising these components.

Battery cycling and parameterisation methods give the series resistance $R_0(T, SOC)$ of a cell. This resistance will decrease monotonically as temperature increases [6, 39, 40]. As a result, a one-to-one mapping emerges between temperature and cell resistance, for a given state-of-charge. By running the mapping in reverse, a cell temperature can be found if the resistance is known. More formally, for temperature T, resistance R_0, and state-of-charge SOC, the inverse mapping is given as

$$T = R_0^{-1}(R_0; SOC) \ , \tag{22}$$

which is illustrated in Fig. 4. This can be exploited to find the effective temperature of a cell, provided its emergent series resistance can be found.

Eq. (21) shows that a heterogeneous cell with temperature profile $T(x_j)$ and state-of-charge profile $SOC(x_j)$ will have an effective series resistance $\tilde{R}_0$ of

$$\tilde{R}_0 = \frac{n_{\text{layer}}}{\sum_{j=1}^{n_{\text{layer}}} \frac{1}{R_0(T_j, SOC_j)}} \ . \tag{23}$$

The inverse mapping can then to find the effective cell temperature, by looking for the temperature that gives the emergent resistance $\tilde{R}_0$. Mathematically, effective temperature T_{eff} is found through the combination of Eq. (22) and (23), as

$$T_{\text{eff}} = R_0^{-1}\left(\frac{n_{\text{layer}}}{\sum_{j=1}^{n_{\text{layer}}} \frac{1}{R_0(T_j, SOC_j)}}; SOC \right) \ . \tag{24}$$

These results can be immediately generalised to a continuous case for $n_{\text{layer}} \to \infty$.

When representing heterogeneous cells with lumped models, the temperature distribution should not be averaged away, as that will lead to incorrect resistance estimates [10]. Nevertheless, Eq. (24) shows that an alternative temperature-averaging method exists, whereby the parts of the cell with the lowest resistance contribute the most weight to the effective cell temperature. Using this, a lumped model

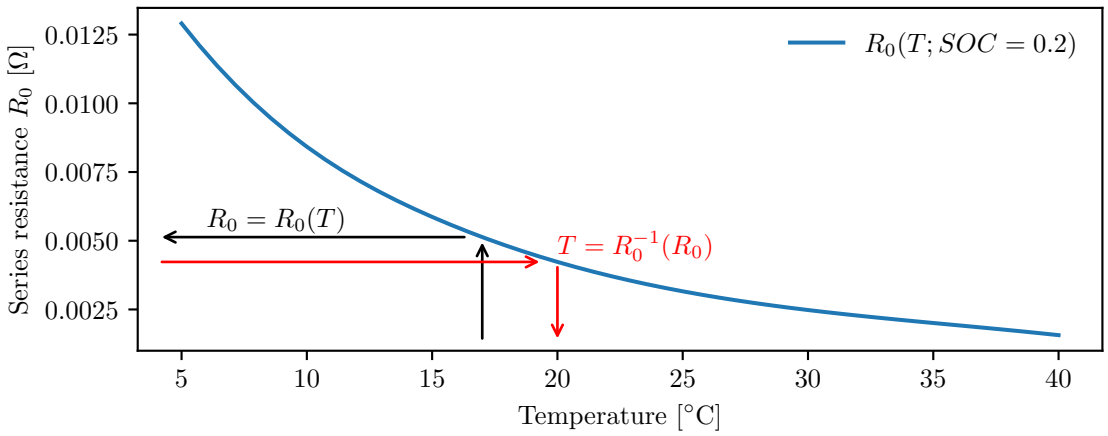

Figure 4: Experimentally obtained resistance, and its inverse function, for R_0 as parameterised in section 2. $R_0(T; SOC)$ maps a temperature T to a resistance R_0, at some given state-of-charge, and its inverse $R_0^{-1}(R_0; SOC)$ maps from resistance back to temperature.

Parameter	Value	
Top heat transfer coefficient	h_0	500 W m^{-2} K^{-1}
Bottom heat transfer coefficient	h_L	0 W m^{-2} K^{-1}
Thermal conductivity	k	1.47 W m^{-1} K^{-1}
Specific heat capacity	c_p	880 J kg^{-1} K^{-1}
Ambient temperature	T_∞	20 °C
Line density	ρ	72.414 kg m^{-1}
Thickness	L	11.6 mm
Nominal capacity	Q_{nom}	42.4 Ah
Number of layers	n_{layer}	20
Number of RC pairs	n_{rc}	2

Table 2: Key parameters for the simulations presented here, derived from [41, 42, 43].

can be set up to show the same resistance as a heterogeneous cell, and therefore, lumped models can be constructed which will show the same electrical performance as a heterogeneous cell, or distributed model. Eq. (24) cannot be used for online estimation problems, as the internal state-of-charge and temperature distributions would not be known; we now show that despite this, effective temperature can still be used reliably for real-world and experimental applications.

3.3 Parameterising thermal models from electrical data recovers effective temperature

So far, a thermal parameterisation method has been proposed and tested experimentally, and effective temperature theory has been developed to infer the lumped operational temperature of a heterogeneous cell. We now tie these two results together, by showing that thermal models parameterised using our methods will predict the effective temperature of a cell. As a result, the temperature predicted by our thermal modelling methods will be the correct and valid choice for real-world usage cases, where heterogeneity will be prevalent. The validation requires knowledge of a cell's internal temperature and state-of-charge distribution, which is difficult to obtain experimentally. Simulations and synthetic data are therefore used here, which enables a more thorough and in-depth analysis than experiments would allow. Heterogeneous cells are simulated using the model in Eqs. (17)–(19), giving heterogeneous-model voltage data $v_{\text{hetero}}(t)$. The methods of section 2 are applied to these data, to parameterise a lumped thermal model. Predictions of both models are then analysed using the effective temperature theory developed in section 3.2.

Simulations are set up to describe commercially relevant cells used in electric vehicles, to highlight the industrial relevance of our methods. Table 2 details the model setup; cell geometry is taken from [41], and thermal parameters from [42, 43]. One side of the model-cell is insulated, and the other is cooled with a

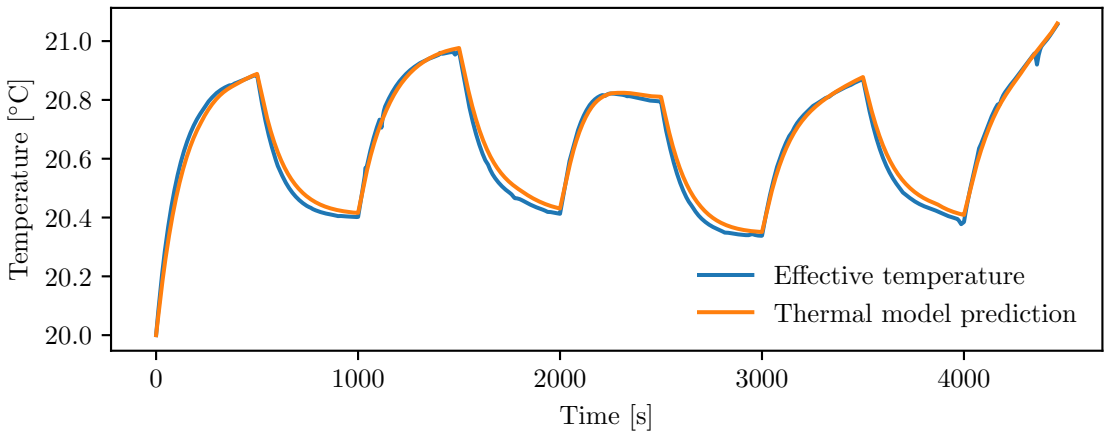

Figure 5: Comparison of calculated effective temperature of a heterogeneous cell, and temperature predictions of a lumped model parameterised entirely from electrical data. The lumped model recovers the effective temperature. This confirms that effective temperature is the correct measure of heterogeneous cell temperature, and demonstrates how it can be recovered from standard cell-cycling tests.

heat transfer coefficient of 500 W m^{-2} K^{-1}, as per section 2.2. Electrical parameters are taken from the previous parameterisation experiments. Cell capacity is scaled to conserve volumetric energy density, and electrical parameters are rescaled accordingly, using resistors and capacitors in parallel arguments. Rescaling and resizing cells and parameters is often performed in the literature [44, 16]. Simulations of the thermal test method are performed, with the current profile and associated voltage trace previously shown in Fig. 3.

As shown in Fig. 5, the thermal model reproduces the effective temperature calculated with Eq. (24). Effective temperature thus emerges naturally from the thermal model calibration, and presents itself as the intrinsic temperature of a heterogeneous cell. This is a notable result since the thermal model is fitted only from current-voltage data, and motivates our claim that effective temperature is the most natural and meaningful temperature measure to use.

To further-validate our methods and illustrate the commercial relevance of our results, we now study the performance of our electrothermal model on an electric vehicle drive-cycle. As before, heterogeneous data are generated using Eq. (17) to allow a full validation against a known effective temperature. Fig. 6 shows that as expected, the lumped thermal model reproduces the effective temperature of the distributed model, despite having not been fitted to any thermal data. Fig. 7 shows the prediction errors of the calibrated model on the same test data. Errors in overpotential prediction are calculated[2] against the heterogeneous data, and compared with a suite of lumped models designed to represent standard modelling methods. For these, model temperature is defined by one of *(i)* the ambient temperature (set-point of the thermal management system); *(ii)* the temperature on the cooled surface of the heterogeneous cell; and *(iii)* the temperature on the insulated surface of the cell. Surface temperatures represent the best-case temperature measurement for operational cells, and would require temperature measurements to be available for each cell in a pack. Nevertheless, these temperature measurements do not represent the cell's effective temperature, and therefore our thermal modelling strategy outperforms the voltage accuracy achieved using instrumented cells. In practice, manufacturers do not instrument each individual cell, due to issues of cost, pack size, and computational burden; instead, temperatures are typically measured on the thermal management system cooling loop. Again, this is not the correct temperature measure for a heterogeneous cell, and as a result our modelling paradigm shows a higher predictive accuracy.

Our lumped modelling method gives a root-mean-square voltage prediction error of 0.48 mV against the heterogeneous simulations, compared to 2.74 mV when the insulated-surface temperature is used, 5.37 mV when the cooled-surface temperature is used, and 9.82 mV for ambient temperature. This indicates that heterogeneous cell dynamics can be modelled accurately with simple and computationally fast lumped models, when effective temperature and voltage-based thermal parameterisation methods

[2]Overpotentials are calculated relative to the 'true' open-circuit voltage $v_{oc}(SOC)$, not the heterogeneous generalisation proposed in Eq. (21).

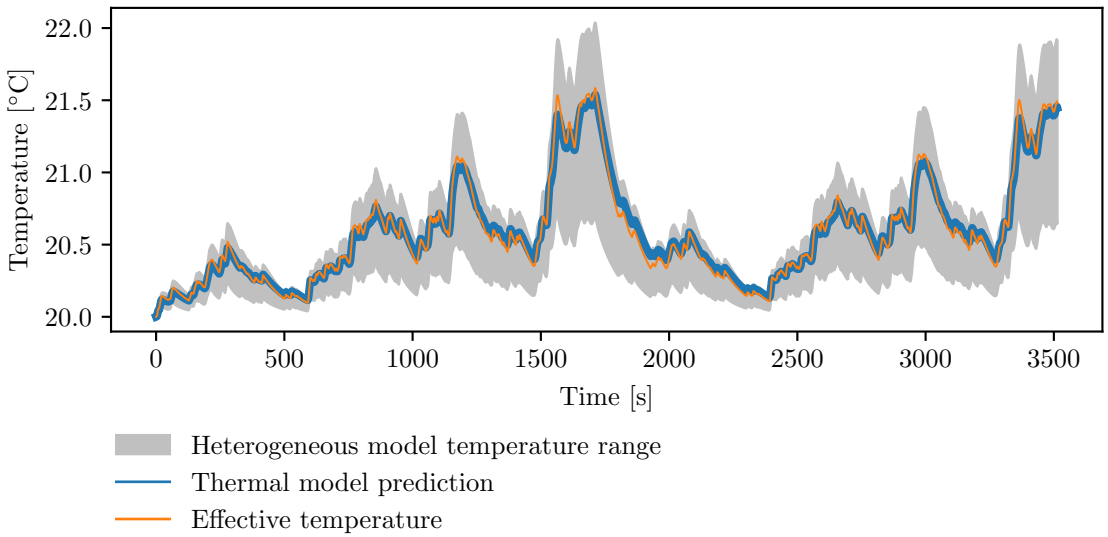

Figure 6: Comparison of temperature predictions for a distributed model, and our calibrated lumped model. Distributed models capture heterogeneity, and exhibit a temperature distribution (grey). Effective temperature can be used as a single temperature measure for this distribution (blue). Our thermal model reproduces cell effective temperature (orange), despite only being fitted to electrical data, reinforcing the validity of both effective temperature and our model parameterisation method.

are used. The small prediction errors that exist between our model and the full heterogeneous data are likely because effective temperature does not account for the small variations in heterogeneous open-circuit voltage, given in Eq. (21).

4 Conclusion

Lumped models are regularly used in battery science, which assume uniformity in properties such as cell temperature and state-of-charge. However, real cells operate with temperature gradients due to their heat generation, which causes a range of knock-on heterogeneous effects. This work demonstrates that despite ignoring temperature gradients, lumped models can generate accurate descriptions of cell electrical behaviours, provided their temperatures are chosen correctly. Accordingly, the 'correct' temperature is defined, and simple experimental methods for thermal parameterisation are developed and shown to yield this temperature.

The effective temperature of a cell is the temperature which a hypothetical, spatially uniform cell would need to be at, to exhibit the same impedance as a heterogeneous cell at the same overall state-of-charge. We provide a formula to calculate effective temperature, which serves as a single, simple temperature measurement that represents the impacts of thermal and state-of-charge gradients on an electrochemical system. A lumped model will be maximally accurate when it operates at the effective temperature of a heterogeneous cell. We develop experiments that enable lumped thermal models to be parameterised from only electrical data. Such data can easily be obtained from a battery cycler, and expensive testing of thermal diffusivity and heat capacity are not required using our methods. Validation work demonstrates that our lumped thermal model is accurate when used with heterogeneous cells, as it predicts the effective temperature of a distributed model. As the thermal predictions are designed to maximise electrical model voltage accuracy, this in turn demonstrates that effective temperature really does maximise electrical problem accuracy. Simulation-based tests show that lumped models using effective temperature provide comparable accuracy to distributed models, and outperforms models using explicit temperature measurements from cells, as these would not capture the effective temperature.

Two ideas for future work are presented. Firstly effective temperature could be investigated for improving the parameterisation of large-format cells, to help correct for the heterogeneity caused by the parameterisation tests. Secondly, the link between a cell's surface and effective temperatures could be explored, with the view of designing advanced state estimation methods which combine surface temperature measurements and effective temperature theory, for maximal estimation accuracy.

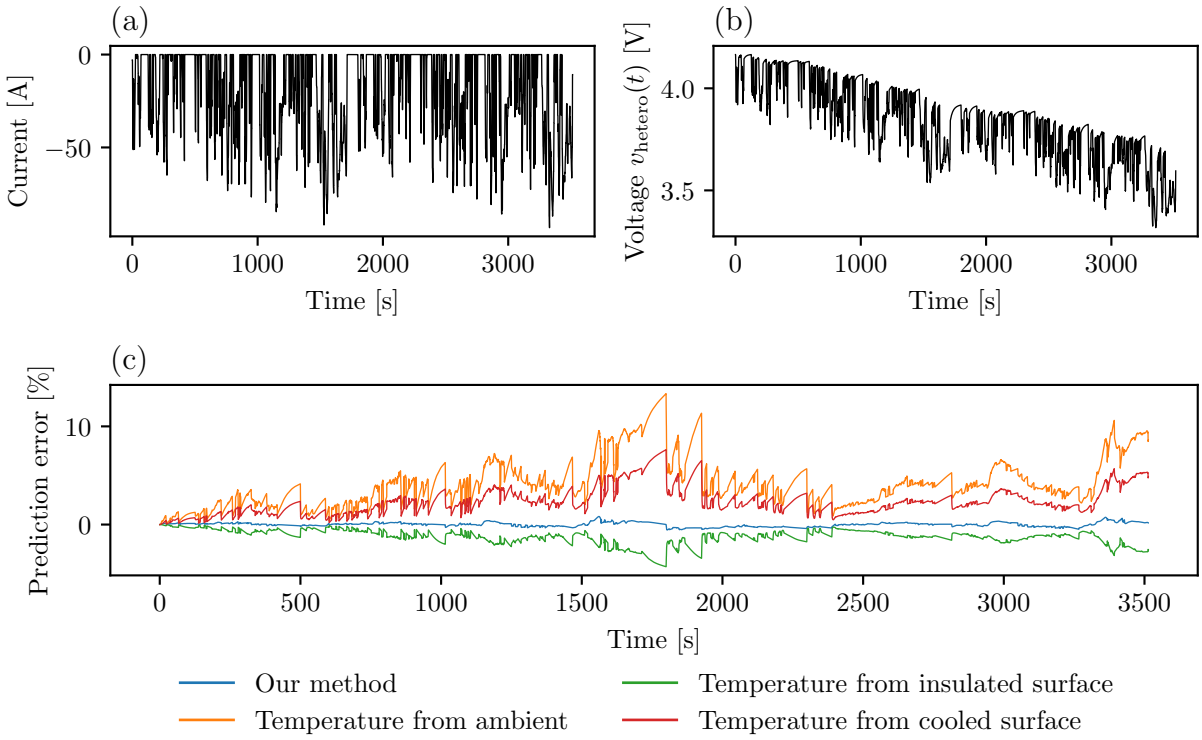

Figure 7: Distributed model simulations using current-based drive-cycle (panel (a)) are used to model voltage responses of a heterogeneous cell (panel (b)). Overpotential prediction errors are calculated against this for a suite of lumped models, taken to represent conventional modelling approaches (panel (c)). Our methods outperform standard modelling approaches, as the calibrated thermal model estimates effective cell temperature, allowing an accurate description of heterogeneous cell behaviours.

Data and code availability

All data and code required to reproduce this manuscript will be made available by request.

Author contributions

Methodology, investigation, software, formal analysis, writing — original draft, visualisation: MB. Conceptualisation, resources: MB, AH. Supervision, writing — review and editing, funding acquisition: AH.

Declaration of interests

The authors declare that they have no conflicts of interest.

Acknowledgements

MB and AH are funded by the Faraday Institution Multi Scale Modelling project (grant number: FIRG059), and two EPSRC IAA projects (grant number: A100419).

References

[1] J. S. Edge, S. O'Kane, R. Prosser, N. D. Kirkaldy, A. N. Patel, A. Hales, A. Ghosh, W. Ai, J. Chen, J. Yang, *et al.*, "Lithium ion battery degradation: what you need to know," *Physical Chemistry Chemical Physics*, vol. 23, no. 14, pp. 8200–8221, 2021.

[2] X. Feng, M. Ouyang, X. Liu, L. Lu, Y. Xia, and X. He, "Thermal runaway mechanism of lithium ion battery for electric vehicles: A review," *Energy storage materials*, vol. 10, pp. 246–267, 2018.

[3] S. Paarmann, K. Schuld, and T. Wetzel, "Inhomogeneous aging in lithium-ion batteries caused by temperature effects," *Energy Technology*, vol. 10, no. 11, p. 2200384, 2022.

[4] S. Li, C. Zhang, Y. Zhao, G. J. Offer, and M. Marinescu, "Effect of thermal gradients on inhomogeneous degradation in lithium-ion batteries," *Communications Engineering*, vol. 2, no. 1, p. 74, 2023.

[5] D. Bernardi, E. Pawlikowski, and J. Newman, "A general energy balance for battery systems," *Journal of the electrochemical society*, vol. 132, no. 1, p. 5, 1985.

[6] M. Alipour, C. Ziebert, F. V. Conte, and R. Kizilel, "A review on temperature-dependent electrochemical properties, aging, and performance of lithium-ion cells," *Batteries*, vol. 6, no. 3, p. 35, 2020.

[7] M. Schönleber, C. Uhlmann, P. Braun, A. Weber, and E. Ivers-Tiffée, "A consistent derivation of the impedance of a lithium-ion battery electrode and its dependency on the state-of-charge," *Electrochimica Acta*, vol. 243, pp. 250–259, 2017.

[8] M. Fleckenstein, O. Bohlen, M. A. Roscher, and B. Bäker, "Current density and state of charge inhomogeneities in li-ion battery cells with lifepo4 as cathode material due to temperature gradients," *Journal of Power Sources*, vol. 196, no. 10, pp. 4769–4778, 2011.

[9] M. P. Klein and J. W. Park, "Current distribution measurements in parallel-connected lithium-ion cylindrical cells under non-uniform temperature conditions," *Journal of The Electrochemical Society*, vol. 164, no. 9, p. A1893, 2017.

[10] Y. Troxler, B. Wu, M. Marinescu, V. Yufit, Y. Patel, A. J. Marquis, N. P. Brandon, and G. J. Offer, "The effect of thermal gradients on the performance of lithium-ion batteries," *Journal of Power Sources*, vol. 247, pp. 1018–1025, 2014.

[11] T. S. Bryden, B. Dimitrov, G. Hilton, C. P. de León, P. Bugryniec, S. Brown, D. Cumming, and A. Cruden, "Methodology to determine the heat capacity of lithium-ion cells," *Journal of Power Sources*, vol. 395, pp. 369–378, 2018.

[12] L. Sheng, L. Su, H. Zhang, Y. Fang, H. Xu, and W. Ye, "An improved calorimetric method for characterizations of the specific heat and the heat generation rate in a prismatic lithium ion battery cell," *Energy Conversion and Management*, vol. 180, pp. 724–732, 2019.

[13] S. Li, S. K. Rawat, T. Zhu, G. J. Offer, and M. Marinescu, "Python-based equivalent circuit network (pyecn) modelling framework for lithium-ion batteries: next generation open-source battery modelling framework for lithium-ion batteries," 2023.

[14] T. G. Tranter, R. Timms, P. R. Shearing, and D. Brett, "Communication—prediction of thermal issues for larger format 4680 cylindrical cells and their mitigation with enhanced current collection," *Journal of The Electrochemical Society*, vol. 167, no. 16, p. 160544, 2020.

[15] Y. Zhao, L. B. Diaz, Y. Patel, T. Zhang, and G. J. Offer, "How to cool lithium ion batteries: optimising cell design using a thermally coupled model," *Journal of The Electrochemical Society*, vol. 166, no. 13, pp. A2849–A2859, 2019.

[16] Y. Zhao, Y. Patel, T. Zhang, and G. J. Offer, "Modeling the effects of thermal gradients induced by tab and surface cooling on lithium ion cell performance," *Journal of The Electrochemical Society*, vol. 165, no. 13, pp. A3169–A3178, 2018.

[17] S. Li, N. Kirkaldy, C. Zhang, K. Gopalakrishnan, T. Amietszajew, L. B. Diaz, J. V. Barreras, M. Shams, X. Hua, Y. Patel, *et al.*, "Optimal cell tab design and cooling strategy for cylindrical lithium-ion batteries," *Journal of Power Sources*, vol. 492, p. 229594, 2021.

[18] R. R. Richardson, P. T. Ireland, and D. A. Howey, "Battery internal temperature estimation by combined impedance and surface temperature measurement," *Journal of Power Sources*, vol. 265, pp. 254–261, 2014.

[19] R. R. Richardson and D. A. Howey, "Sensorless battery internal temperature estimation using a kalman filter with impedance measurement," *IEEE Transactions on Sustainable Energy*, vol. 6, no. 4, pp. 1190–1199, 2015.

[20] R. R. Richardson, S. Zhao, and D. A. Howey, "On-board monitoring of 2-d spatially-resolved temperatures in cylindrical lithium-ion batteries: Part ii. state estimation via impedance-based temperature sensing," *Journal of Power Sources*, vol. 327, pp. 726–735, 2016.

[21] R. Richardson, *Impedance-based battery temperature monitoring*. PhD thesis, University of Oxford, 2016.

[22] S. S. Madani, E. Schaltz, and S. Knudsen Kær, "Review of parameter determination for thermal modeling of lithium ion batteries," *Batteries*, vol. 4, no. 2, p. 20, 2018.

[23] S. S. Madani, C. Ziebert, and M. Marzband, "Thermal behavior modeling of lithium-ion batteries: A comprehensive review," *Symmetry*, vol. 15, no. 8, p. 1597, 2023.

[24] Y. Ye, Y. Shi, N. Cai, J. Lee, and X. He, "Electro-thermal modeling and experimental validation for lithium ion battery," *Journal of Power Sources*, vol. 199, pp. 227–238, 2012.

[25] G. L. Plett, *Battery management systems, Volume I: Battery modeling*. Artech House, 2015.

[26] N. Tian, Y. Wang, J. Chen, and H. Fang, "One-shot parameter identification of the thevenin's model for batteries: Methods and validation," *Journal of Energy Storage*, vol. 29, p. 101282, 2020.

[27] M. Lagraoui, M. Lhayani, A. Nejmi, and A. Abbou, "A new method for identifying the parameters of the li-ion battery thevenin model," in *2024 4th International Conference on Innovative Research in Applied Science, Engineering and Technology (IRASET)*, pp. 1–5, IEEE, 2024.

[28] M. Hossain, S. Saha, M. E. Haque, M. T. Arif, and A. M. T. Oo, "A parameter extraction method for the thevenin equivalent circuit model of li-ion batteries," in *2019 IEEE Industry Applications Society Annual Meeting*, pp. 1–7, IEEE, 2019.

[29] S. Jiang, "A parameter identification method for a battery equivalent circuit model," tech. rep., SAE Technical Paper, 2011.

[30] R. Jackey, M. Saginaw, P. Sanghvi, J. Gazzarri, T. Huria, and M. Ceraolo, "Battery model parameter estimation using a layered technique: an example using a lithium iron phosphate cell," tech. rep., SAE Technical Paper, 2013.

[31] J. Knox, M. Blyth, and A. Hales, "Advancing state estimation for lithium-ion batteries with hysteresis through systematic extended kalman filter tuning," *Scientific Reports*, vol. 14, no. 1, p. 12472, 2024.

[32] T. Zhu, R. Tomlin, C. Garcia, S. Rawat, T. Holland, G. Offer, and M. Marinescu, "Lithium-ion battery model parametrisation: Batpar an all-in-one toolkit for equivalent circuit models," *Journal of Energy Storage*, vol. 92, p. 112220, 2024.

[33] B. Planden, N. E. Courtier, M. Robinson, A. Khetarpal, F. B. Planella, and D. A. Howey, "Pybop: A python package for battery model optimisation and parameterisation," *arXiv preprint arXiv:2412.15859*, 2024.

[34] C. Roe, X. Feng, G. White, R. Li, H. Wang, X. Rui, C. Li, F. Zhang, V. Null, M. Parkes, *et al.*, "Immersion cooling for lithium-ion batteries–a review," *Journal of Power Sources*, vol. 525, p. 231094, 2022.

[35] T. Bruen and J. Marco, "Modelling and experimental evaluation of parallel connected lithium ion cells for an electric vehicle battery system," *Journal of Power Sources*, vol. 310, pp. 91–101, 2016.

[36] R. Arunachala, C. Parthasarathy, A. Jossen, and J. Garche, "Inhomogeneities in large format lithium ion cells: A study by battery modelling approach," *ECS Transactions*, vol. 73, no. 1, p. 201, 2016.

[37] S. Hamdi, W. E. Schiesser, and G. W. Griffiths, "Method of lines," *Scholarpedia*, vol. 2, no. 7, p. 2859, 2007.

[38] M. Crescentini, A. De Angelis, R. Ramilli, G. De Angelis, M. Tartagni, A. Moschitta, P. A. Traverso, and P. Carbone, "Online eis and diagnostics on lithium-ion batteries by means of low-power integrated sensing and parametric modeling," *IEEE Transactions on Instrumentation and Measurement*, vol. 70, pp. 1–11, 2020.

[39] D. Andre, M. Meiler, K. Steiner, C. Wimmer, T. Soczka-Guth, and D. Sauer, "Characterization of high-power lithium-ion batteries by electrochemical impedance spectroscopy. i. experimental investigation," *Journal of Power Sources*, vol. 196, no. 12, pp. 5334–5341, 2011.

[40] S. Hossain Ahmed, X. Kang, and S. Bade Shrestha, "Effects of temperature on internal resistances of lithium-ion batteries," *Journal of energy resources technology*, vol. 137, no. 3, p. 031901, 2015.

[41] Y. Xie, A. Hales, R. Li, X. Feng, Y. Patel, and G. Offer, "Thermal management optimization for large-format lithium-ion battery using cell cooling coefficient," *Journal of The Electrochemical Society*, vol. 169, no. 11, p. 110511, 2022.

[42] G. White, A. Hales, Y. Patel, and G. Offer, "Novel methods for measuring the thermal diffusivity and the thermal conductivity of a lithium-ion battery," *Applied Thermal Engineering*, vol. 212, p. 118573, 2022.

[43] K. O'Regan, F. B. Planella, W. D. Widanage, and E. Kendrick, "Thermal-electrochemical parameters of a high energy lithium-ion cylindrical battery," *Electrochimica Acta*, vol. 425, p. 140700, 2022.

[44] S. Al Hallaj, H. Maleki, J.-S. Hong, and J. R. Selman, "Thermal modeling and design considerations of lithium-ion batteries," *Journal of power sources*, vol. 83, no. 1-2, pp. 1–8, 1999.